Asian Journal of Chemistry; Vol. 38, No. 7 (2026), 1785-1794
ASIAN JOURNAL OF CHEMISTRY
https://doi.org/10.14233/ajchem.2026.35801

Fish Scale-Derived Biosorbent from *Tenualosa ilisha* for the Removal of Congo Red Dye from Aqueous Solutions: Isotherms, Thermodynamics and Kinetics

SANANDA MALANGI[1], UMME SULTANA LIMA[1], MD. KORBAN ALI[2], MAHMUDUL HASSAN SUHAG[1] and MD. NAZMUL KAYES[1,*]

[1]Department of Chemistry, University of Barishal, Barishal 8254, Bangladesh
[2]Department of Chemistry, Jashore University of Science and Technology, Jashore 7408, Bangladesh

*Corresponding author: E-mail: dmnkayes@bu.ac.bd

Received: 22 February 2026 *Accepted*: 27 May 2026 *Published online*: 3 July 2026 AJC-22404

In this work, the potential of fish scales from *Tenualosa ilisha* (TIFS) as a sustainable bio-adsorbent for removing Congo red (CR) dye from an aqueous solution is reported. The adsorption was carried out in an electric shaker to evaluate the effect of adsorbent dosages, initial dye concentration, pH and temperature. A UV-visible spectrophotometer was used to monitor the adsorption capacity of TIFS. Almost all the CR molecules (99.84%) were adsorbed on the surface of TIFS at a CR concentration of 8×10^{-5} M, 3 g of TIFS, 26 ºC temperature, pH = 9.65 and a contact time of 50 min. FTIR analysis confirmed the involvement of functional groups such as hydroxyl and amide in the adsorption process. SEM images revealed significant morphological changes on the TIFS surface after adsorption, while EDX analysis showed increased nitrogen and oxygen contents, indicating successful dye uptake. The experimental results indicate that CR adsorption on the surface of TIFS is an exothermic process. Based on thermodynamic inspection, negative values of Gibbs free energy (ΔG) suggested a spontaneous adsorption process. The adsorption of CR on TIFS is found to follow Freundlich adsorption isotherm and pseudo-second order kinetics.

Keywords: Adsorption, Congo red, Fish scales, Isotherm, Kinetics, Thermodynamics.

INTRODUCTION

The protection of surface and groundwater resources has become a critical environmental challenge due to the increasing discharge of industrial, agricultural and urban wastewater containing dyes, heavy metals and pharmaceutical contaminants [1]. Among various industries, the textile sector is a major contributor to water pollution through the release of effluents containing toxic substances such as arsenic, cadmium, copper, lead, chromium, nickel, mercury, sulphur compounds and auxiliary chemicals that pose serious risks to ecological and human health [2]. Textile dyes discharged into aquatic systems increase biochemical oxygen demand (BOD) and chemical oxygen demand (COD), thereby reducing water quality and inhibiting the growth of aquatic organisms [3]. Globally, the textile industry consumes more than 10,000 tons of dyes annually, a significant fraction of which ultimately enters water bodies [4]. Exposure to these dyes may cause respiratory disorders, allergic reactions and other adverse health effects in humans [5].

A substantial proportion of dyes applied during textile processing remains unfixed and is subsequently released into wastewater streams. Azo dyes are of particular concern since they reduce water transparency, restrict light penetration and impair photosynthetic activity, resulting in oxygen depletion and disruption of aquatic ecosystems [5-7]. Moreover, many azo dyes and their degradation products exhibit toxic, mutagenic and carcinogenic properties, adversely affecting aquatic organisms, soil microorganisms and environmental quality [5,8]. Congo red (CR), a benzidine-based anionic diazo dye, possesses a highly stable aromatic structure containing two azo linkages, making it resistant to biodegradation and persistent in aquatic environments [4,9]. Owing to its toxicity and potential carcinogenicity, efficient removal of Congo red from wastewater is essential before effluent discharge [4,9].

Various treatment technologies, including ion-exchange, membrane separation, chemical precipitation, coagulation-flocculation and oxidation-reduction, have been employed for removal of dyes. However, these methods often suffer from high operational costs, incomplete pollutant removal and sludge generation [10]. In contrast, adsorption has emerged as an attractive alternative due to its simplicity, cost-effectiveness, high removal efficiency and ease of adsorbent regeneration, making it a sustainable approach for wastewater treatment applications [11,12].

The effectiveness, simplicity of preparation and low cost of adsorption by conventional adsorbents and biosorbents are reasons for their increasing relevance [13-15]. Plant leaves have been used over time to make biosorbents for the purification of water [16], fruit shells [17], tree barks [18], spent tea leaves [19], banana peel [20], coconut shell [21], sawdust [22], mango leaves [23], chitosan [24], egg shell [25], fish scales [26] and other biomaterials. Among them, activated carbon [27] and nanostructured materials [28] are widely used adsorbents for wastewater treatment due to their high surface area and strong adsorption capacity toward heavy metals and organic pollutants. Although activated carbon possesses excellent porosity and extensive surface area, its non-selective nature limits its effectiveness toward small or highly polar organic molecules. Similarly, nanomaterials exhibit enhanced surface activity and adsorption efficiency due to their high surface free energy, enabling the removal of heavy metals, dyes, oily wastes and other industrial contaminants [29]. However, the synthesis of these advanced adsorbents often requires sophisticated technologies, resulting in high production and operational costs. In contrast, fish scales represent an inexpensive, sustainable and eco-friendly biosorbent derived from abundant biological waste, offering a value-added approach for wastewater remediation.

Recent years have witnessed growing interest in the utilisation of fish scales as natural adsorbents due to their low cost, widespread availability and excellent adsorption potential [30-35]. Composed primarily of collagen and hydroxyapatite, fish scales provide numerous active sites for pollutant binding and have shown promising performance in the removal of various dyes from aqueous media [36]. For example, adsorption studies of acid blue 121 using fish scale-derived hydroxyapatite demonstrated optimum removal at pH 2.0, dye concentration of 100 mg L^{-1}, temperature of 30 ºC and adsorbent dosage of 1.0 g L^{-1}, with the adsorption process fitting the Langmuir isotherm model [37]. Kinetic investigations further revealed that the adsorption behaviour was best described by the pseudo-second-order model, indicating strong interactions between the dye molecules and the adsorbent surface [38]. Similarly, Rohu (*Labeo rohita*) fish scales effectively removed brilliant red dye, achieving maximum adsorption at pH 7.2 and exhibiting Langmuir-type adsorption behaviour with an exothermic adsorption energy of -34.92 kJ mol^{-1} [39].

Motivated by these findings, the present study explores the potential of *Tenualosa ilisha* fish scales (TIFS) as a biosorbent for the removal of Congo red (CR) dye from aqueous solutions. *Tenualosa ilisha*, the national fish of Bangladesh, accounts for more than 80% of global production, making its scales an abundant and readily available waste resource. The study systematically investigates the influence of key operational parameters, including adsorbent dosage, dye concentration, solution pH, temperature and contact time, on Congo red removal efficiency. Furthermore, adsorption equilibrium, kinetic and thermodynamic models were employed to elucidate the adsorption mechanism and evaluate the feasibility of TIFS as a sustainable biosorbent for wastewater treatment.

EXPERIMENTAL

Preparation of fish scales: The fish scales of *T. ilisha* were collected, cleaned and dried at 60 ºC in an oven. To achieve a consistent particle size, the dried scales were crushed and sieved.

Preparation of Congo red solution: A stock solution of Congo red (CR) dye was prepared by dissolving an appropriate amount of Congo red (m.f.: $C_{32}H_{22}N_6Na_2O_6S_2$; *m.w.*: 696.664 g mol^{-1}, λ_{max} = 498 nm) in distilled water to obtain a concentration of 1×10^{-2} M in a 250 mL volumetric flask. The pH of the dye solutions was adjusted and monitored within the range of 2.0-8.0 using a calibrated digital pH meter. The working solutions of the desired concentrations were subsequently prepared by serial dilution of the stock solution with distilled water.

Adsorption study and characterisation of adsorbent: A specific quantity of fish scales was added to a CR solution and allowed to shake in a shaker. After a predetermined amount of time, a small portion of the solution was collected. The absorbance of each solution was measured with a double-beam UV-visible spectrophotometer (Shimadzu-1900i) and the removal efficiency was measured. Distilled water was used as a reference for all measurements. The process was repeated with the modification of various parameters, including the dosage of the adsorbent, the concentration of the adsorbate, contact time, pH and temperature. The percentage of adsorption was determined by eqn. 1:

$$\text{Adsorption } (\%) = \frac{\text{Abs}_{\text{initial}} - \text{Abs}_{\text{final}}}{\text{Abs}_{\text{initial}}} \times 100 \qquad (1)$$

The functional groups of fish scales (FS) before and after adsorption were characterised using FTIR spectroscopy in the range of 4000-400 cm^{-1}.

RESULTS AND DISCUSSION

The maximum absorption wavelength (λ_{max}) of aqueous Congo red (CR) solution was determined spectrophotometrically as 498 nm, with a molar extinction coefficient (ε) of 2.352×10^4 L mol^{-1} cm^{-1}. All adsorption experiments were monitored at this wavelength, and the ε value was used for calculating adsorption isotherm, kinetic and thermodynamic parameters.

Effect of adsorbent doses: As shown in Fig. 1, the adsorption efficiency of CR initially increased with increasing adsorbent dosage, reached a maximum and subsequently decreased when the dosage was further increased while keeping all other parameters constant. The adsorption efficiency increased steadily up to 3 g of fish scale adsorbent, attaining a maximum removal of 99.84%. This improvement can be

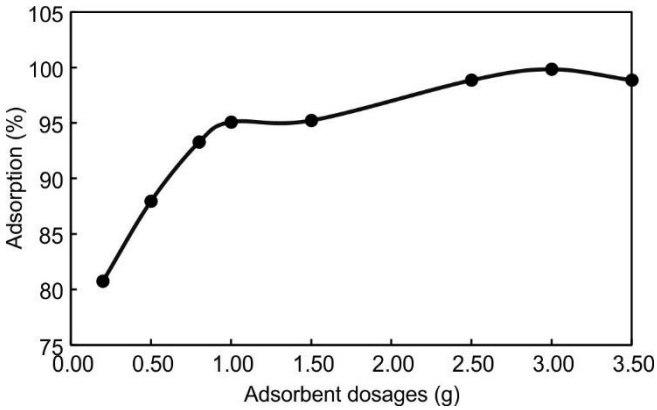

Fig. 1. Percentage of adsorption at various adsorbent dosage [$[CR]_o$ = 8 × 10^{-5} M, pH = 9.65, t = 60 min, T = 26 ºC]

attributed to the higher availability of active adsorption sites and increased surface area for dye uptake [40]. The adsorbent dosage plays a crucial role in determining adsorption performance because it directly influences the adsorbate-adsorbent equilibrium and the number of accessible binding sites [41]. However, at dosages exceeding 3 g, a decrease in adsorption efficiency was observed, which may be attributed to particle aggregation and overcrowding effects that reduce the effective surface area and cause overlapping of adsorption sites, thereby limiting dye adsorption [42]. Consequently, 3 g was identified as the optimum adsorbent dosage for the removal of CR using fish scale adsorbent.

Effect of dye concentration: The effect of the initial Congo red concentration on adsorption efficiency is shown in Fig. 2. The dye concentration was varied from 8 × 10^{-5} M to 16 × 10^{-5} M while maintaining all other experimental parameters constant. The adsorption efficiency decreased from 99.84% to 92.84% with increasing dye concentration. At lower concentrations, a large number of active adsorption sites are available relative to the number of dye molecules, resulting in higher removal efficiency. As the initial dye concentration increases, the number of dye molecules competing for the limited adsorption sites also increases, leading to a reduction in percentage removal [43,44].

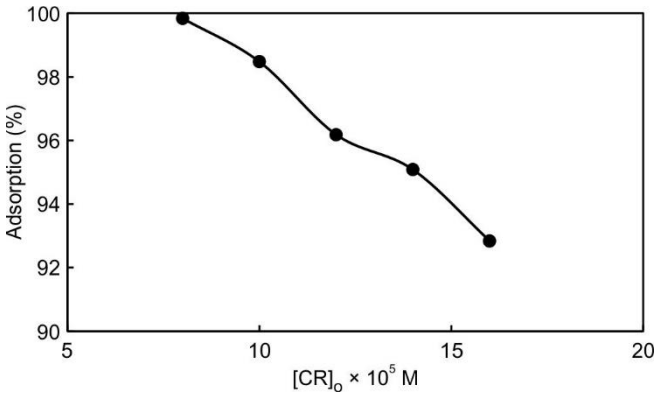

Fig. 2. Percentage of adsorption at different concentration of CR [amount of TIFS = 3 g, pH = 9.65, t = 50 min, T = 26 ºC]

The initial dye concentration serves as an important driving force for mass transfer between the aqueous phase and the adsorbent surface. However, at higher concentrations, the available active sites gradually become saturated, limiting further adsorption and reducing removal efficiency [44]. Although the absolute amount of dye adsorbed may increase at higher concentrations, the percentage removal generally decreases due to insufficient adsorption sites relative to the increased dye load [45]. The observed decrease in adsorption efficiency at increased CR concentrations can therefore be attributed to surface saturation and increased competition among dye molecules for the available binding sites on the fish scale adsorbent [46].

Effect of pH: The pH of the solution is a key parameter influencing the adsorption process, as it affects both the surface charge of the adsorbent and the ionization state of the adsorbate. The effect of pH on CR adsorption was investigated over the pH range of 6-11 using 1 M HCl and 1 M NaOH for pH adjustment. In each experiment, 100 mL of Congo red solution was treated with 3.0 g of *T. ilisha* fish scale (TIFS) adsorbent for 60 min. The results (Fig. 3) demonstrate that adsorption efficiency is strongly pH-dependent. The maximum CR removal was achieved at pH 9.65, which was therefore selected as the optimum pH for subsequent experiments. The enhanced adsorption at this pH may be attributed to favorable electrostatic interactions and the zwitterionic nature of the dye molecules. A decrease in adsorption efficiency was observed when the pH was increased beyond 9.65, likely due to changes in the surface charge of the adsorbent and increased competition from hydroxyl ions, which reduce the availability of active adsorption sites [47]. Similarly, at lower pH values, protonation of surface functional groups and dye molecules may weaken adsorbent-adsorbate interactions, resulting in reduced adsorption efficiency. Consequently, the removal efficiency decreased as the pH deviated from the optimum value of 9.65 toward either acidic or strongly alkaline conditions.

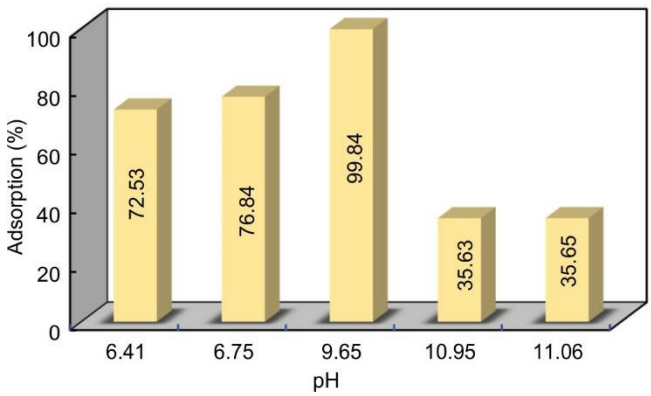

Fig. 3. Effect of pH on the percentage of adsorption [amount of TIFS = 3 g, $[CR]_o$ = 8 × 10^{-5} M, t = 50 min, T = 26 ºC]

Effect of temperature: According to adsorption theory, adsorption generally decreases with increasing temperature since adsorbed molecules tend to desorb from the adsorbent surface at elevated temperatures [48]. Since adsorption is typically an exothermic process, lower temperatures favour dye uptake, in accordance with Le Chatelier's principle. As the temperature increases, the kinetic energy of the adsorbate molecules rises, promoting desorption and reducing the extent of adsorption [49]. As shown in Fig. 4, the adsorption

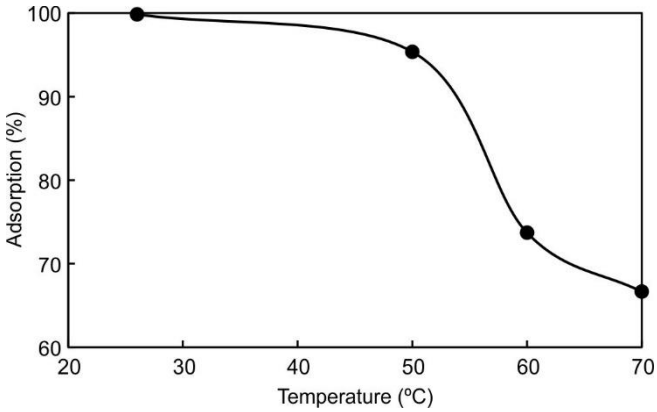

Fig. 4. Percentage of adsorption at various temperature [amount of TIFS = 3 g, $[CR]_o = 8 \times 10^{-5}$ M, t = 50 min, pH = 9.65]

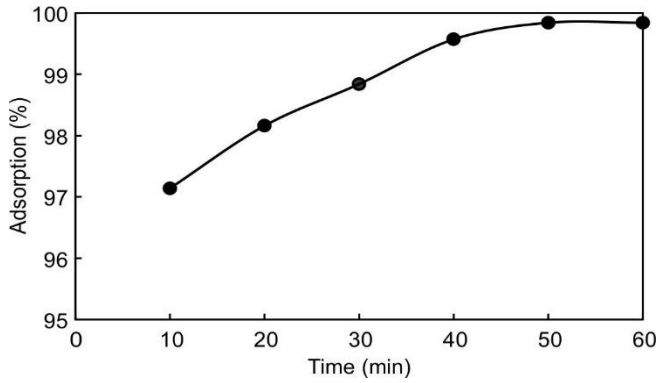

Fig. 5. Effect of contact time on the percentage of adsorption [amount of TIFS = 3 g, $[CR]_o = 8 \times 10^{-5}$ M, pH = 9.65, T = 26 ºC]

efficiency of CR decreased with increasing temperature from 26 ºC to 80 ºC, indicating the exothermic nature of the adsorption process. The highest adsorption efficiency was observed at 26 ºC (room temperature), while elevated temperatures led to a progressive decline in dye removal due to enhanced desorption and possible reduction in the availability of active binding sites.

Effect of contact time: The effect of contact time for CR removal by *T. ilisha* fish scales (TIFS) was investigated over a period of 0-60 min using 3.0 g of adsorbent in 100 mL of dye solution. As shown in Fig. 5, the adsorption efficiency increased with increasing contact time due to the progressive occupation of available active sites on the biosorbent surface [50]. The percentage removal increased from 97.14% to 99.84% as the contact time was extended from 10 to 50 min. Beyond 50 min, no significant change in absorbance or adsorption efficiency was observed, indicating that adsorption equilibrium had been attained. This suggests that nearly all available adsorption sites were occupied by dye molecules at 50 min, establishing it as the optimum contact time for CR adsorption onto TIFS.

FTIR spectra analysis: FTIR spectroscopy was used to investigate the functional groups involved in the adsorption of CR onto TIFS. The FTIR spectrum of CR (Fig. 6a) exhibited a broad band around 3400 cm^{-1} corresponding to O–H/N–H stretching vibrations, a prominent peak near 1600 cm^{-1} assigned to aromatic C=C stretching and N–H bending vibrations and characteristic sulphonate ($-SO_3^-$) stretching bands at approximately 1185 and 1045 cm^{-1} [43,51]. These functional groups are primarily responsible for the interaction of CR molecules with the adsorbent surface.

The FTIR spectrum of TIFS before adsorption (Fig. 6b) displayed a broad O–H stretching band in the region 3600-3200 cm^{-1}, along with characteristic amide-I (~1650 cm^{-1}) and amide-II (~1550 cm^{-1}) bands arising from the collagen matrix. After adsorption, noticeable changes in the intensity and position of these bands were observed, indicating the involvement of hydroxyl, amide and phosphate groups in the adsorption process. The reduction in O–H band intensity suggests hydrogen-bond formation between TIFS and CR molecules, while shifts in the amide bands indicate interactions between collagen functional groups and the dye molecules. Furthermore, changes in the 1250-1000 cm^{-1} region suggest the participation of phosphate groups through ion-exchange or complexation mechanisms [43,51]. Thus, the FTIR results confirm that adsorption of Congo red onto TIFS occurs through a combination of hydrogen bonding, electrostatic attraction and possible π-π interactions between the functional groups of the dye and the collagen-rich fish scale surface, demonstrating the effectiveness of TIFS as a sustainable biosorbent for CR dye removal.

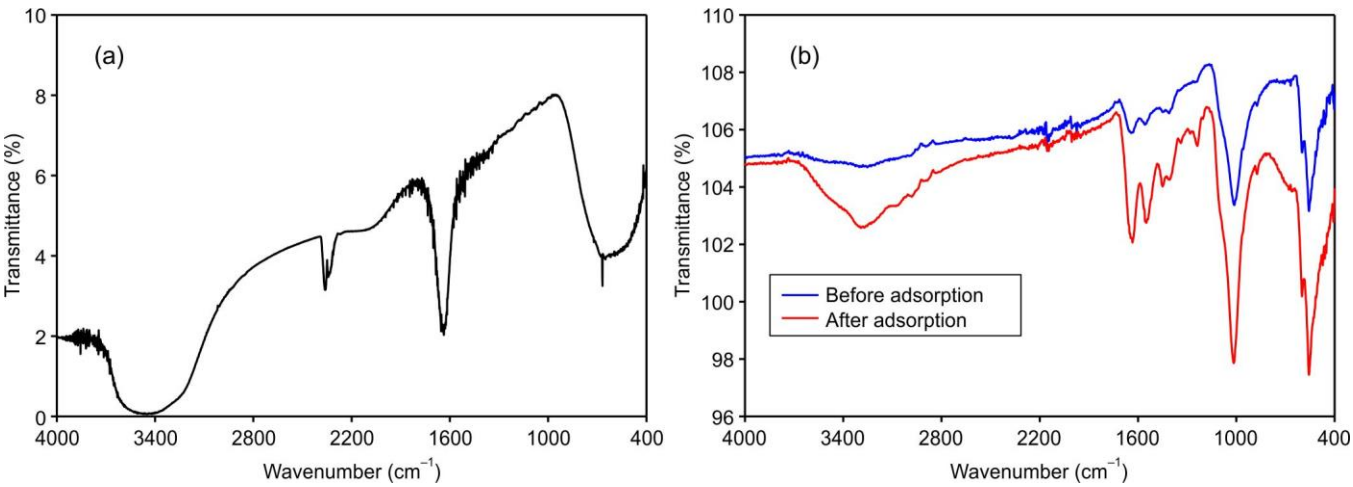

Fig. 6. FTIR spectra analysis of (a) CR and (b) TIFS before (blue) and after (red) adsorption of CR

Surface morphology and elemental analysis: SEM analysis of TIFS revealed significant morphological transformations subsequent to CR adsorption. Before adsorption, micrographs in Fig. 7a exhibited a characteristically fibrous and microporous structure, featuring clear ridges and uneven surfaces that support adsorption by increasing surface area and making active sites more accessible. After adsorption imaging in Fig. 7b showed clear changes in surface structure, including more uneven texture, blocked pores and the presence of unstructured particles, which are signs that the dye had attached to the surface, likely forming a single layer [52].

Energy-dispersive X-ray spectroscopy (EDX) was employed to examine elemental changes on the surface of TIFS before and after CR adsorption. The EDX spectrum of pristine TIFS (Fig. 8a) revealed the presence of carbon (25.43%), oxygen (31.44%), calcium (28.66%), phosphorus (11.40%) and nitrogen (3.07%), confirming the hydroxyapatite and collagen-rich composition of the biosorbent. Following CR adsorption (Fig. 8b), the oxygen and nitrogen contents increased to 40.00% and 5.93%, respectively, while the carbon content decreased to 17.08%. These changes indicate the successful attachment of CR molecules containing nitrogen-bearing azo and amino groups as well as oxygen-rich sulphonate functionalities onto the biosorbent surface. Furthermore, the decrease in the Ca/P ratio from 2.51 to 2.38 suggests the involvement of hydroxyapatite-associated phosphate groups in the adsorption process. The observed elemental variations support the FTIR findings and confirm that both the collagen and hydroxyapatite components of TIFS contribute synergistically to the adsorption of CR dye [53].

Adsorption kinetics: Adsorption kinetics describes the rate at which adsorbate molecules are transferred from the aqueous phase to the adsorbent surface and provides valuable information regarding the adsorption mechanism and rate-controlling steps. Kinetic studies are commonly evaluated using both linear and non-linear models and the most appropriate model is identified based on the goodness-of-fit parameters [54]. In this study, the adsorption kinetics of CR onto TIFS were analysed using established kinetic models. The pseudo-first-order kinetic model, also known as the Lagergren model, assumes that the rate of adsorption is proportional to the number of unoccupied adsorption sites and that the adsorption rate depends on the difference between the equilibrium adsorption capacity and the amount adsorbed at a given time [55,56]. The model is represented by the following equation:

$$\frac{dq_t}{dt} = k_1 - (q_e - q_t) \quad (2)$$

where q_e is the adsorption capacity of adsorbent at equilibrium (mg g^{-1}); q_t is the adsorption capacity of the adsorbent at time t (mg g^{-1}), k_1 is the rate constant for pseudo-first-order adsorption (min^{-1}).

After eqn. 2 is integrated and boundary conditions are applied, t = 0 to t = t and q_t = 0 to $q_t = q_e$, the integrated form of eqn. 1 becomes:

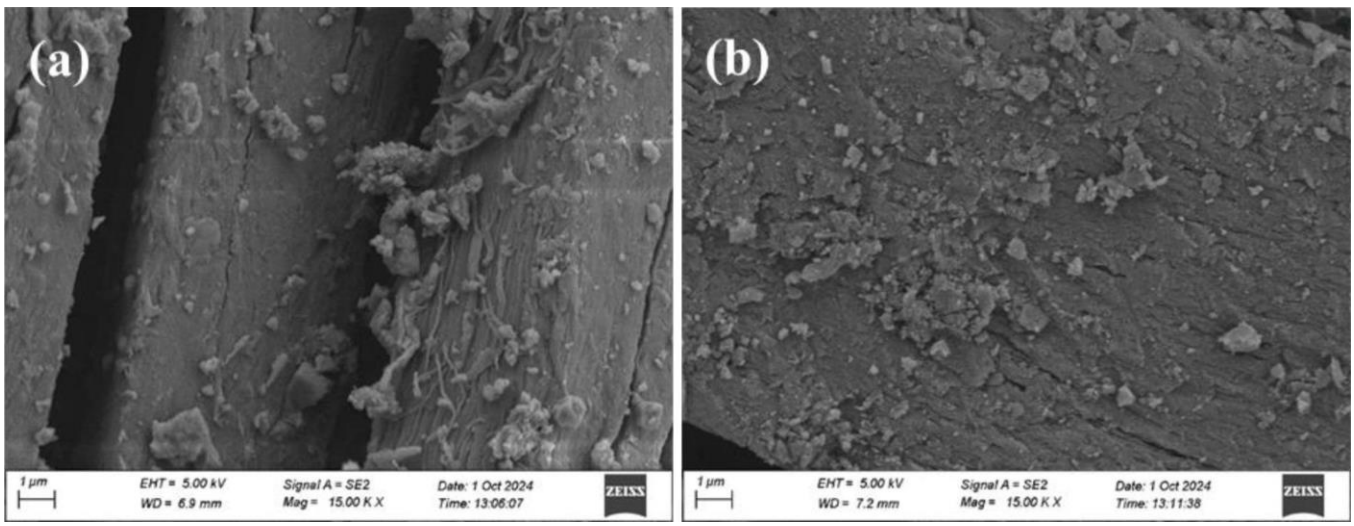

Fig. 7. SEM images of TIFS (a) before adsorption and (b) after adsorption of CR

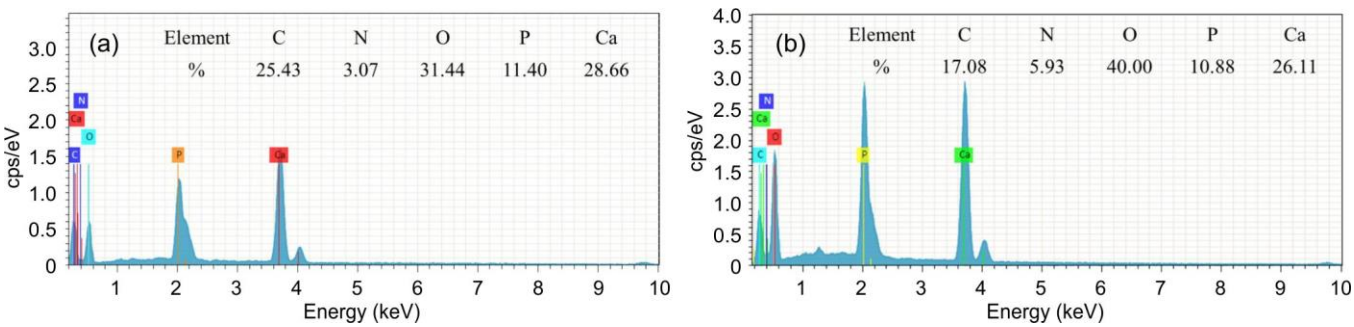

Fig. 8. EDX spectra of TIFS (a) before adsorption and (b) after adsorption of CR

$$\log(q_e - q_t) = \log q_e - k_1 t \quad (3)$$

when values of ln ($q_e - q_t$) were correlated linearly with t. The plot of log ($q_e - q_t$) *versus* t gives a relationship that is linear from which k_1 and q_e can be determined from the slope and intercept of the plot.

The adsorption kinetics rate equation for pseudo-second-order [57] is expressed as:

$$\frac{dq_t}{dt} = k_2(q_e - q_t)^2 \quad (4)$$

where k_2 is the rate constant of pseudo-second order adsorption (g mg^{-1} min^{-1}).

The integrated form of the equation for the boundary conditions t = 0 to t = t and q_t = 0 to $q_t = q_e$ becomes:

$$\frac{1}{(q_e - q_t)} = \frac{1}{q_e} + kt \quad (5)$$

The equation is linearly rearranged and expressed as:

$$\frac{t}{q_t} = \frac{1}{k_2 q_e^2} + \frac{t}{q_e} \quad (6)$$

Based on the adsorption capacity, Ho & McKay [58] analyses the pseudo-second-order kinetic model, which is represented as follows:

$$\frac{t}{q_t} = \frac{1}{h} + \frac{t}{q_e} \quad (7)$$

$$h = k_2 q_e^2 \quad (8)$$

where h (mg g^{-1} min^{-1}) is the initial adsorption rate, k_2 (g mg^{-1} min^{-1}) is the equilibrium rate constant of pseudo-second order model. The values of q_e and k_2 were calculated from the slope and intercept of the graph drawn between t/q_t and t, respectively.

The value of q_e and q_t were calculated by using the following equations [59]:

$$q_t = \frac{(C_o - C_t)V}{W} \quad (9)$$

$$q_e = \frac{(C_o - C_e)V}{W} \quad (10)$$

where C_0 and C_e, C_t represents the initial and equilibrium concentration of dye in mg/L respectively. V is the volume of the solution (L) used for adsorption and W is the mass of dry adsorbent (g).

The kinetic parameters were determined from the graph in Fig. 9 by using pseudo-first and pseudo-second order models and given in Table-1. The correlation coefficient (R^2) values suggest that the adsorption of CR on TIFS follow pseudo-second order kinetics.

TABLE-1
KINETIC PARAMETERS FOR THE PSEUDO-FIRST AND PSEUDO-SECOND ORDER MODELS

q_e (mg/g)	Pseudo-first order		Pseudo-second order	
	k_1	R^2	k_2	R^2
1.83	0.0527	0.7907	1.0585	0.9999

Adsorption isotherms: To determine the best-fitting equilibrium model for CR adsorption onto TIFS, the experimental data were analyzed using Langmuir, Freundlich, Temkin and Dubinin-Radushkevich (D–R) isotherms. The Langmuir isotherm assumes monolayer adsorption on a homogeneous surface with a finite number of identical adsorption sites and no interaction between adsorbed molecules [60]. The linear form of the Langmuir equation is given as:

$$\frac{1}{q_e} = \frac{1}{q_{max} K_L C_e} + \frac{1}{q_{max}} \quad (11)$$

where K_L is the Langmuir adsorption constant (L mg^{-1}) and q_{max} represents the theoretical maximum adsorption capacity (mg g^{-1}) [61].

The Freundlich isotherm is established on the multilayer adsorption (heterogeneous surface). The linearised form of Freundlich isotherm is given as:

$$\ln q_e = \ln K_F + \frac{1}{n} \ln C_e \quad (12)$$

where the isotherm constants K_F (L mg^{-1}) and 'n' indicate the capacity and intensity of the adsorption, respectively [62].

The linearised form of Temkin isotherm equation can be expressed by the following equation:

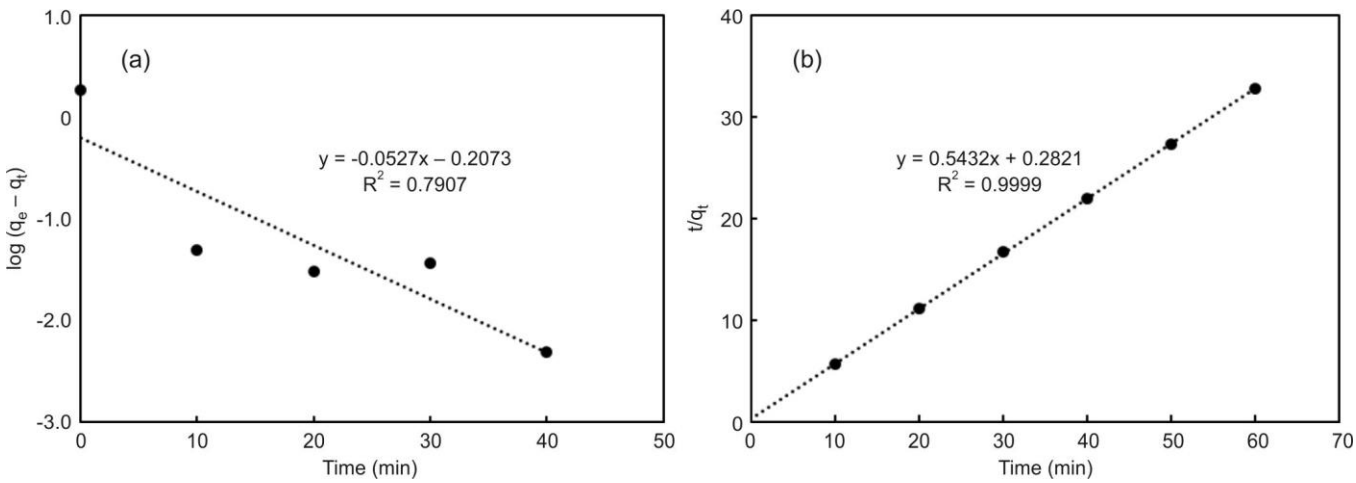

Fig. 9. (a) Pseudo-first order and (b) pseudo-second order kinetic model for the adsorption of CR on TIFS

$$q_e = B\ln K_T + B\ln C_e \quad (13)$$

where T is the absolute temperature in K; R is the universal gas constant, 8.314 J K^{-1} mol^{-1}; K_T is the equilibrium binding constant (L mg^{-1}); and B is related to the heat of adsorption [63].

The linear form of Dubinin–Radushkevich isotherm equation can be expressed as:

$$\ln q_e = \ln q_{max} - \beta\varepsilon^2 \quad (14)$$

where q_{max} is the DR monolayer capacity (mg g^{-1}), β is a constant related to adsorption energy and ε is the Polanyi potential, which is related to the equilibrium concentration as follows [62]:

$$\varepsilon = RT\ln\left(1+\frac{1}{C_e}\right) \quad (15)$$

The mean free energy (E) of adsorption per molecule of the adsorbate when it is shifted to the surface of the solid from infinity in the solution can be determined from the value of β [64].

The data fitting of the Langmuir, Freundlich, Temkin and Dubinin–Radushkevich isotherms on the adsorption of CR onto TIFS are shown in Fig. 10. The parameters of all the isotherms with the correlation coefficients for the adsorption of CR onto TIFS are tabulated in Table-2. Based on the correlation coefficient (R^2), the Freundlich model isotherm represents a better fit compared to the other isotherm models with the experimental data. The results illustrate the heterogeneity of the adsorbent surface involving multilayer adsorption [65]. Generally, the value of 1/n, ranging between 0 and 1 represents favourable adsorption conditions. The value of 1/n is obtained 0.13 from Table-2, which indicates that the adsorption of CR on TIFS is favourable [66].

Adsorption thermodynamics: Several thermodynamic parameters, including Gibbs free-energy change (ΔG°), enthalpy change (ΔH°) and entropy change (ΔS°) were estimated to inspect the adsorption nature of the present work.

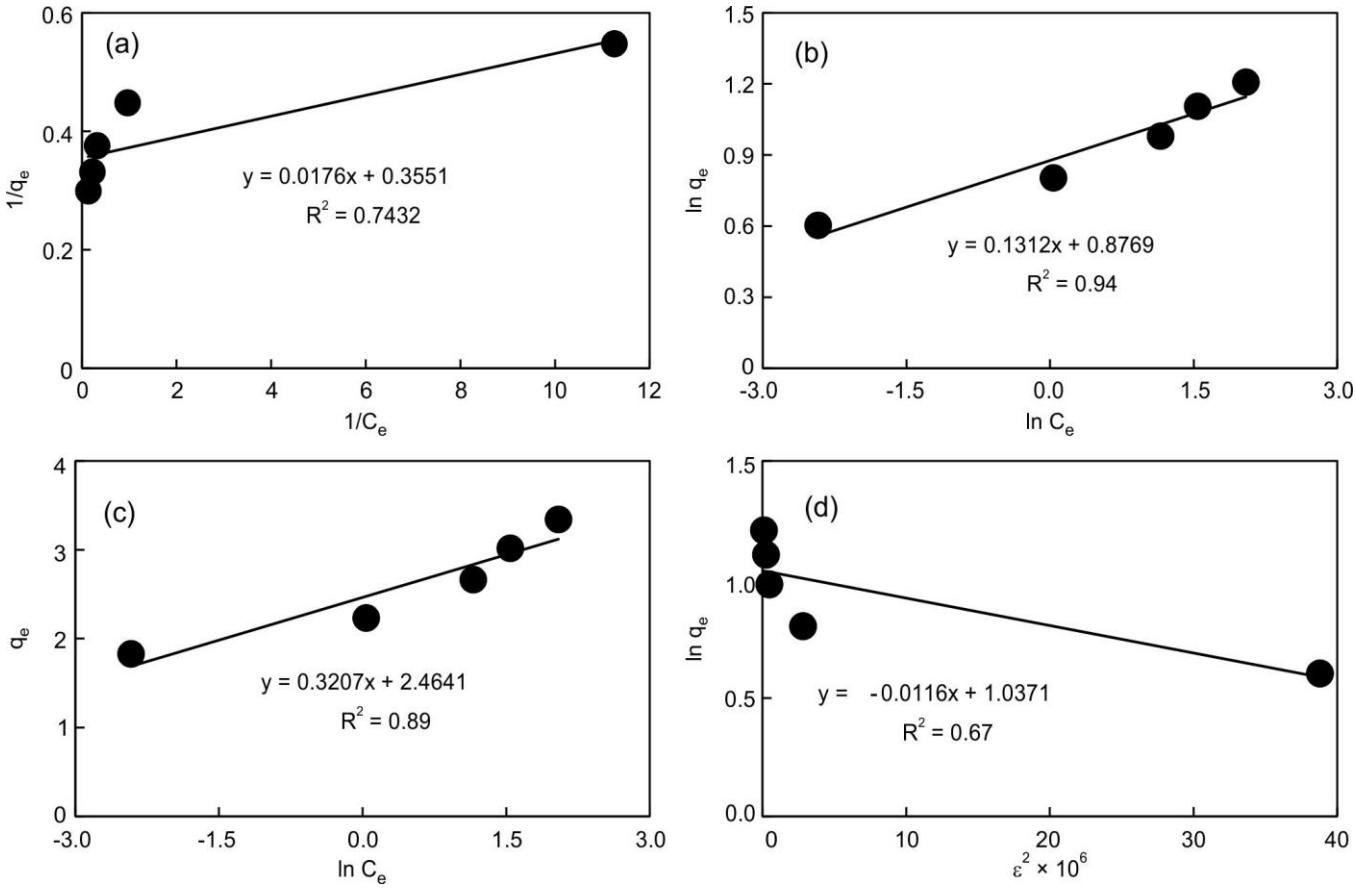

Fig. 10. (a) Langmuir, (b) Freundlich, (c) Temkin and (d) Dubinin–Radushkevich isotherms of the adsorption of CR onto TIFS

TABLE-2
ADSORPTION ISOTHERM PARAMETERS AND CORRELATION COEFFICIENTS OF CR ADSORPTION ONTO TIFS

Isotherm models				
Langmuir	K_L (L mg^{-1}): 20.18	q_{max} (mg g^{-1}): 2.82		R^2: 0.74
Freundlich	K_F (L mg^{-1}): 2.40	1/n: 0.13	n: 7.62	R^2: 0.94
Temkin	K_T (L mg^{-1}): 2172.22	B: 0.32		R^2: 0.89
Dubinin-Radushkevich	β: 1.16×10^{-8}	q_{max} (mg g^{-1}): 2.82	E (KJ mol^{-1}): 6.6×10^3	R^2: 0.67

The Gibbs free energy change (ΔG^o) is computed by the following equation:

$$\Delta G^o = -RT \ln k_d = -RT \ln \frac{q_e}{C_e} \quad (17)$$

where R is the universal gas constant (8.3145 J mol^{-1} K^{-1}); T is the temperature (K); K_d is the distribution coefficient (L g^{-1}); q_e is the equilibrium amount of adsorbed molecule on the adsorbent TIFS (mg g^{-1}) and C_e is the equilibrium concentration of CR dye in the aqueous phase (mg L^{-1}) [67].

As shown in Fig. 11, the equilibrium amount of adsorbed molecule (q_e) on the adsorbent TIFS is increased, as well as the Gibbs free energy change at standard state (ΔG^o) is also increased with increasing temperature, demonstrating the decrement of adsorption with increasing temperature. Furthermore, the negative values of ΔG^o at 26 ºC suggested that the adsorption of CR solution onto TIFS was a spontaneous process at ambient temperature. The values of ΔG^o become positive at other higher temperatures indicating that the adsorption becomes non-spontaneous with increasing temperature from ambient conditions (Fig. 11 and Table-3).

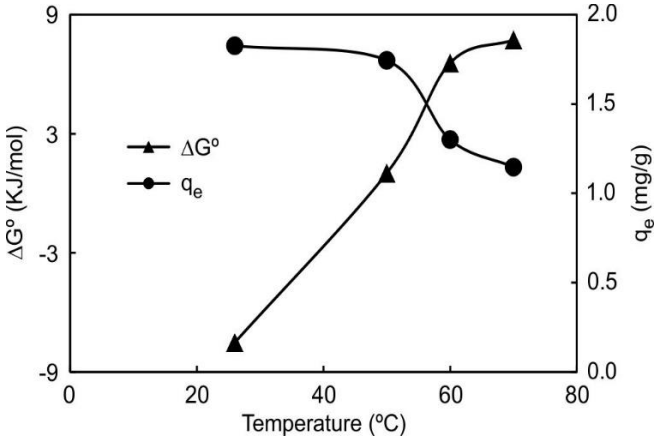

Fig. 11. The relationship between temperature and amount of CR dye (8×10^{-5} M) adsorbed, q_e on TIFS and corresponding Gibbs free energy change (ΔG^o)

TABLE-3
THERMODYNAMIC PARAMETERS FOR ADSORPTION OF CONGO RED (CR) DYE ON TIFS

Temp. (ºC)	Gibbs free energy change (ΔG^o) (KJ mol^{-1})	Enthalpy change (ΔH^o) (KJ mol^{-1})	Entropy change (ΔS^o) (KJ mol^{-1})
26	-7.51	-116.87	-3.66
50	1.02		
60	6.56		
70	7.73		

The van't Hoff equation can be implied to explain the relationship between enthalpy change and entropy change as follows:

$$\ln k_d = \frac{\Delta S^o}{R} - \frac{\Delta H^o}{RT} \quad (18)$$

As illustrated in Fig. 12, the values of ΔH^o and ΔS^o were determined from the slope and intercept of ln K_d *vs.* 1/T plots [61,62]. The values of the estimated thermodynamic parameters are presented in Table-3. The negative value of ΔH^o (-116.87 KJ mol^{-1}) revealed the exothermic nature of the adsorption procedure, the negative ΔS^o value (-3.66 kJ mol^{-1}) indicates a decrease in molecular randomness and disorder at the solid-liquid interface after the adsorption of CR onto TIFS [61].

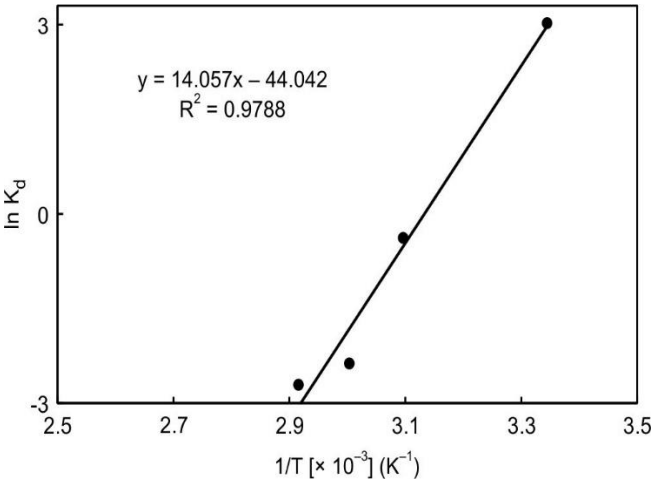

Fig. 12. The plot of ln K_d *versus* 1/T

Conclusion

This study demonstrated the potential of discarded *Tenualosa ilisha* fish scales (TIFS) as an efficient, sustainable and low-cost biosorbent for the removal of Congo red (CR) dye from aqueous solutions. Batch adsorption experiments revealed that dye removal was significantly influenced by adsorbent dosage, initial dye concentration, pH, temperature and contact time. Under optimized conditions (3 g adsorbent, pH 9.65, 26 ºC and 50 min contact time), a maximum removal efficiency of 99.84% was achieved. The adsorption efficiency decreased at higher dye concentrations and temperatures, indicating saturation of active sites and the exothermic nature of the process. Thermodynamic parameters confirmed that adsorption was spontaneous and exothermic (ΔH^o = -116.87 kJ mol^{-1}; $\Delta G^o < 0$). FTIR, SEM and EDX analyses verified the involvement of hydroxyl, amide and phosphate groups in dye adsorption and revealed significant surface and elemental changes after adsorption. Kinetic and isotherm studies suggested that the adsorption process was predominantly governed by chemisorption and occurred on a heterogeneous surface with multilayer adsorption characteristics. Based on the results, TIFS represent a promising biosorbent for the efficient and eco-friendly treatment of dye-contaminated wastewater.

CONFLICT OF INTEREST

The authors declare that there is no conflict of interests regarding the publication of this article.

DECLARATION OF AI-ASSISTED TECHNOLOGIES

During the preparation of this manuscript, the authors used an AI-assisted tool(s) to improve the language. The authors reviewed and edited the content and take full responsibility for the published work.

REFERENCES

1. Z. Jeirani, C.H. Niu and J. Soltan, *Rev. Chem. Eng.*, **33**, 491 (2017); https://doi.org/10.1515/revce-2016-0027
2. A.K. Al-Buriahi, A.A. Al-Gheethi, P. Senthil Kumar, R.M.S. Radin Mohamed, H. Yusof, A.F. Alshalif and N.A. Khalifa, *Chemosphere*, **287**, 132162 (2022); https://doi.org/10.1016/j.chemosphere.2021.132162
3. B. Lellis, C.Z. Fávaro-Polonio, J.A. Pamphile and J.C. Polonio, *Biotechnol. Res. Innov.*, **3**, 275 (2019); https://doi.org/10.1016/j.biori.2019.09.001
4. R. Ahmad and R. Kumar, *Appl. Surf. Sci.*, **257**, 1628 (2010); https://doi.org/10.1016/j.apsusc.2010.08.111
5. M.A. Hassaan and A. El Nemr, *Egypt. J. Aquatic Res.*, **43**, 1 (2017); https://doi.org/10.1016/j.ejar.2016.11.002
6. L.C. Apostol, L. Pereira, R. Pereira, M. Gavrilescu and M.M. Alves, *Biodegradation*, **23**, 725 (2012); https://doi.org/10.1007/s10532-012-9548-7
7. B. Manu and S. Chaudhari, *Process Biochem.*, **38**, 1213 (2003); https://doi.org/10.1016/S0032-9592(02)00291-1
8. D. Goswami, J. Mukherjee, C. Mondal and B. Bhunia, *Sci. Total Environ.*, **954**, 176426 (2024); https://doi.org/10.1016/j.scitotenv.2024.176426
9. F. Fu and Q. Wang, *J. Environ. Manage.*, **92**, 407 (2011); https://doi.org/10.1016/j.jenvman.2010.11.011
10. S. Dutta, B. Gupta, S.K. Srivastava and A.K. Gupta, *Mater. Adv.*, **2**, 4497 (2021); https://doi.org/10.1039/D1MA00354B
11. T.A. Aragaw and F.M. Bogale, *Front. Environ. Sci.*, **9**, 764958 (2021); https://doi.org/10.3389/fenvs.2021.764958
12. K.H. Hama Aziz, N.M. Fatah and K.T. Muhammad, *R. Soc. Open Sci.*, **5**, 232033 (2024); https://doi.org/10.1098/rsos.232033
13. I. Ali, *Chem. Rev.*, **112**, 5073 (2012); https://doi.org/10.1021/cr300133d
14. A.G. Adeniyi and J.O. Ighalo, *J. Environ. Chem. Eng.*, **7**, 103100 (2019); https://doi.org/10.1016/j.jece.2019.103100
15. O. Eletta, J.O. Ighalo and O.A.A. Eletta, *J. Res. Inf. Civ. Eng.*, **16**, 2479 (2019).
16. I. Anastopoulos, A. Robalds, D. Mitrogiannis, D.A. Giannakoudakis, H.N. Tran, A. Hosseini-Bandegharaei and G.L. Dotto, *Environ. Chem. Lett.*, **17**, 755 (2019); https://doi.org/10.1007/s10311-018-00829-x
17. M.A. Alghamdi, E.M. Bakhsh, T.M. Fagieh, A.S. Almaghrabi, K. Akhtar and S.B. Khan, *Desalin. Water Treatment*, **326**, 101748 (2026); https://doi.org/10.1016/j.dwt.2026.101748
18. S. Fauzia, H. Aziz, D. Dahlan and R. Zein, *AIP Conf. Proc.*, **2023**, 020081 (2018); https://doi.org/10.1063/1.5064078
19. F. Nabilah Daski and N.A. Ab. Aziz, *IOP Conf. Ser. Earth Environ. Sci.*, **1022**, 012066 (2022); https://doi.org/10.1088/1755-1315/1022/1/012066
20. K.C.S. Farias, R.C.A. Guimarães, K.R.W. Oliveira, C.E.D. Nazário, J.A.P. Ferencz and H. Wender, *Toxics*, **11**, 664 (2023); https://doi.org/10.3390/toxics11080664
21. A. Qisti, Y. Utomo and D.A. Rokhim, *Fuller. J. Chem.*, **6**, 7 (2021); https://doi.org/10.37033/fjc.v6i1.213
22. D. Politi and D. Sidiras, *Procedia Eng.*, **42**, 1969 (2012); https://doi.org/10.1016/j.proeng.2012.07.593
23. G. Vyavahare, P. Jadhav, J. Jadhav, R. Patil, C. Aware, D. Patil, A. Gophane, Y.H. Yang and R. Gurav, *J. Clean. Prod.*, **207**, 296 (2019); https://doi.org/10.1016/j.jclepro.2018.09.193
24. J. Lopez-Cervantes, R.G. Sanchez-Duarte, D.I. Sanchez-Machado, M.A. Correa-Murrieta, J.A. Nunez-Gastelum and J.R. Rodriguez-Nunez, *Environ. Eng. Manag. J.*, **15**, 2469 (2016); https://doi.org/10.30638/eemj.2016.270
25. R.G. Saratale, Q. Sun, V.S. Munagapati, G.D. Saratale, J. Park and D.S. Kim, *Chemosphere*, **281**, 130777 (2021); https://doi.org/10.1016/j.chemosphere.2021.130777
26. A. Bukhari, Z. Hassan, M. Atta, A. Nazir, F. Aslam, A. Naouar, F.F. Al-Fawzan, S.A. Alissa, M. Iqbal and N. Ahmad, *Adsorpt. Sci. Technol.*, **2022**, 5395720 (2022); https://doi.org/10.1155/2022/5395720
27. J.B. Njewa and V.O. Shikuku, *Appl. Surf. Sci. Adv.*, **18**, 100501 (2023); https://doi.org/10.1016/j.apsadv.2023.100501
28. W.S. Choi and H.-J. Lee, *Polymers*, **14**, 2183 (2022); https://doi.org/10.3390/polym14112183
29. H.D. Beyene and T.G. Ambaye, in eds.: Inamuddin, S. Thomas, R. K. Mishra and A. M. Asiri, Application of Sustainable Nanocomposites for Water Purification Process, In: Sustainable Polymer Composites and Nanocomposites, Cham, Springer International Publishing, pp. 387-412 (2019).
30. S. Chakraborty, S. Chowdhury and P.D. Saha, *J. Water Reuse Desalin.*, **2**, 175 (2012); https://doi.org/10.2166/wrd.2012.074
31. R. Bhaumik, N.K. Mondal and S. Chattoraj, *J. Fluor. Chem.*, **195**, 57 (2017); https://doi.org/10.1016/j.jfluchem.2017.01.015
32. K. Zhu, X. Gong, D. He, B. Li, D. Ji, P. Li, Z. Peng and Y. Luo, *RSC Adv.*, **3**, 25221 (2013); https://doi.org/10.1039/c3ra43817a
33. A. Jaafar, A. Darchen, A. Driouich, Z. Lakbaibi, A. Boussaoud, B. Chatib, Y. Laftani, M. El Makhfouk and M. Hachkar, *Inorg. Chem. Commun.*, **137**, 109196 (2022); https://doi.org/10.1016/j.inoche.2022.109196
34. S.M. Javad Sajjadi Shourije, P. Dehghan, M.E. Bahrololoom, A.J. Cobley, V. Vitry, G.T. Pourian Azar, H. Kamyab and M. Mesbah, *Chemosphere*, **317**, 137829 (2023); https://doi.org/10.1016/j.chemosphere.2023.137829
35. N. Nerdy, P. Lestari, D. Simorangkir, V. Aulianshah, F. Yusuf and T.K. Bakri, *Int. J. Appl. Pharm.*, **14**, 181 (2022); https://doi.org/10.22159/ijap.2022v14i2.43560
36. I.G. Shaikhiev, S.V. Sverguzova, R.Z. Galimova and A.S. Grechina, *IOP Conf. Ser. Mater. Sci. Eng.* **945**, 012044 (2020); https://doi.org/10.1088/1757-899X/945/1/012044
37. D. Uzunoğlu and A. Özer, *Desalination Water Treat.*, **57**, 14109 (2016); https://doi.org/10.1080/19443994.2015.1063091
38. N.G. Ahmadgurabi, A. Dadvand Koohi and A.E. Pirbazari, *J. Water Environ. Nanotechnol.*, **3**, 219 (2018); https://doi.org/10.22090/jwent.2018.03.003
39. H.A. Begum and M.H. Kabir, *Dhaka Univ. J. Sci.*, **61**, 7 (2013); https://doi.org/10.3329/dujs.v61i1.15089
40. B. Sumalatha, Y. Prasanna Kumar, K. Kiran Kumar, D. John Babu, A. Venkata Narayana, K. Maria Das and T.C. Venkateswarulu, *Res. J. Pharm. Biol. Chem. Sci.*, **5**, 912 (2014).
41. W.C. Wanyonyi, J.M. Onyari and P.M. Shiundu, *Energy Procedia*, **50**, 862 (2014); https://doi.org/10.1016/j.egypro.2014.06.105
42. E. Bernard, A. Jimoh and J.O. Odigure, *Res. J. Chem. Sci.*, **3**, 3 (2013).
43. S. Banerjee and M.C. Chattopadhyaya, *Arab. J. Chem.*, **10**, S1629 (2017); https://doi.org/10.1016/j.arabjc.2013.06.005
44. F. Doulati Ardejani, K. Badii, F. Farhadi, M. Aziz Saberi and B. Jodeiri Shokri, *Environ. Model. Assess.*, **17**, 505 (2012); https://doi.org/10.1007/s10666-012-9310-x
45. M.N. Kayes, M.J. Miah, M. Obaidullah, M.A. Hossain and M.M. Hossain, *J. Adv. Chem*, **12**, 4127 (2016).
46. H.B.Z. Mohamad Zulfika, R. Baini and N.S. Ahmad Zauzi, *IOP Conf. Ser. Mater. Sci. Eng.* **205**, 012026 (2017); https://doi.org/10.1088/1757-899X/205/1/012026
47. K. Litefti, M.S. Freire, M. Stitou and J. González-Alvarez, *Sci. Rep.*, **9**, 16530 (2019); https://doi.org/10.1038/s41598-019-53046-z
48. M. Horsfall Jnr. and A.I. Spiff, *Electron. J. Biotechnol.*, **8**, 162 (2005); https://doi.org/10.2225/vol8-issue2-fulltext-4

49. R.A. Miah, M.J. Alam, A. Khatun, M.H. Suhag and M.N. Kayes, *J. Eng. Adv.*, **3**, 6 (2022); https://doi.org/10.38032/jea.2022.01.002
50. E. Demirbas, M. Kobya and M.T. Sulak, *Bioresour. Technol.*, **99**, 5368 (2008); https://doi.org/10.1016/j.biortech.2007.11.019
51. R. Lafi, I. Montasser and A. Hafiane, *Adsorpt. Sci. Technol.*, **37**, 160 (2019); https://doi.org/10.1177/0263617418819227
52. G.O. Achieng, C.O. Kowenje, J.O. Lalah and S.O. Ojwach, *Water Sci. Technol.*, **80**, 2218 (2019); https://doi.org/10.2166/wst.2020.040
53. S.M.F. Kabir, R. Cueto, S. Balamurugan, L.D. Romeo, J.T. Kuttruff, B.D. Marx and I.I. Negulescu, *Cleanroom Technol.*, **1**, 311 (2019); https://doi.org/10.3390/cleantechnol1010021
54. Y. Musah, J. Suleiman, A. Mann, E.Y. Shaba and A. Andaliyu, *Biol. Environ. Sci. J. Trop.*, **15**, 1 (2018).
55. J. Zhou, S. Yang, J. Yu and Z. Shu, *J. Hazard. Mater.*, **192**, 1114 (2011); https://doi.org/10.1016/j.jhazmat.2011.06.013
56. U.A. Edet and A.O. Ifelebuegu, *Processes*, **8**, 665 (2020); https://doi.org/10.3390/pr8060665
57. F.T. Ademiluyi and J.C. Nze, *Int. J. Res. Eng. Technol.*, **5**, 164 (2016); https://doi.org/10.15623/ijret.2016.0501033
58. Y.S. Ho and G. McKay, *Process Biochem.*, **34**, 451 (1999); https://doi.org/10.1016/S0032-9592(98)00112-5
59. G. Vijayakumar, R. Tamilarasan and M. Dharmendirakumar, *J. Mater. Environ. Sci.*, **3**, 157 (2012).
60. P.C. Nwadibia, J.C. Eze, D.I. Anyaogu, H.O. Abugu and P.M. Ejikeme, *Discov. Chem.*, **2**, 152 (2025); https://doi.org/10.1007/s44371-025-00233-9
61. M.H. Suhag, A. Khatun, I. Tateishi, M. Furukawa, H. Katsumata and S. Kaneco, *RSC Adv.*, **14**, 17888 (2024); https://doi.org/10.1039/D4RA01481B
62. N. Akter, M.A. Hossain, M.J. Hassan, M.K. Amin, M. Elias, M.M. Rahman, A.M. Asiri, I.A. Siddiquey and M.A. Hasnat, *J. Environ. Chem. Eng.*, **4**, 1231 (2016); https://doi.org/10.1016/j.jece.2016.01.013
63. M. Maria Rahman, N. Akter, M.R. Karim, N. Ahmad, M.M. Rahman, I.A. Siddiquey, N.M. Bahadur and M.A. Hasnat, *J. Environ. Chem. Eng.*, **2**, 76 (2014); https://doi.org/10.1016/j.jece.2013.11.023
64. C. Gerente, V.K.C. Lee, P. Le Cloirec and G. McKay, *Crit. Rev. Environ. Sci. Technol.*, **37**, 41 (2007); https://doi.org/10.1080/10643380600729089
65. S. Swaminathan, N. Imayathamizhan and A. Muthumanickkam, *J. Elastomers Plast.*, **53**, 48 (2021); https://doi.org/10.1177/0095244319897284
66. V.K. Gupta, R. Kumar, A. Nayak, T.A. Saleh and M.A. Barakat, *Adv. Colloid Interface Sci.*, **193-194**, 24 (2013); https://doi.org/10.1016/j.cis.2013.03.003
67. L. Yan, H. Gao and Y. Chen, *ACS Appl. Nano Mater.*, **4**, 7746 (2021); https://doi.org/10.1021/acsanm.1c01035